

# Nitrogen Atom Transfer Catalysis by Metallonitrene C–H Insertion: Photocatalytic Amidation of Aldehydes

Till Schmidt-Räntsch, Hendrik Verplancke, Jonas N. Lienert, Serhiy Demeshko, Matthias Otte, Gerard P. Van Trieste, III, Kaleb A. Reid, Joseph H. Reibenspies, David C. Powers,\* Max C. Holthausen,\* and Sven Schneider\*

In memory of Professor Ulf Diederichsen

**Abstract:** C–H amination and amidation by catalytic nitrene transfer are well-established and typically proceed via electrophilic attack of nitrenoid intermediates. In contrast, the insertion of (formal) terminal nitride ligands into C–H bonds is much less developed and catalytic nitrogen atom transfer remains unknown. We here report the synthesis of a formal terminal nitride complex of palladium. Photocrystallographic, magnetic, and computational characterization support the assignment as an authentic metallonitrene (Pd–N) with a diradical nitrogen ligand that is singly bonded to Pd<sup>I</sup>. Despite the subvalent nitrene character, selective C–H insertion with aldehydes follows nucleophilic selectivity. Transamidation of the benzamide product is enabled by reaction with N<sub>3</sub>SiMe<sub>3</sub>. Based on these results, a photocatalytic protocol for aldehyde C–H trimethylsilylamidation was developed that exhibits inverted, nucleophilic selectivity as compared to typical nitrene transfer catalysis. This first example of catalytic C–H nitrogen atom transfer offers facile access to primary amides after deprotection.

## Introduction

Catalytic nitrene insertion into C–H bonds has emerged as a versatile synthetic methodology for secondary amines and amides.<sup>[1]</sup> Organic azides are attractive N–R sources to generate the reactive key intermediates with significant nitrenoid character, M←N–R.<sup>[2,3]</sup> Mechanistic studies support generally electrophilic reactivity of the subvalent nitrogen ligands either via concerted or radical rebound C–H insertion pathways.<sup>[4,5]</sup> The use of metal nitride complexes in principle offers a complementary strategy to generate primary nitrogenous products. However, such *nitrogen atom transfer* is far less developed. Stoichiometric N-atom transfer of nitride complexes to olefins has been applied in synthesis,<sup>[6]</sup> and reported in solution for some electrophilic nitrides or upon nitride activation with Lewis acids.<sup>[7,8]</sup> Likewise, direct nitride insertion into C–H bonds is rare, particularly intermolecular examples (Scheme 1).<sup>[9,10,11]</sup> Furthermore, radical rebound mechanisms can suffer from the

[\*] T. Schmidt-Räntsch, Dr. S. Demeshko, Dr. M. Otte, Prof. S. Schneider

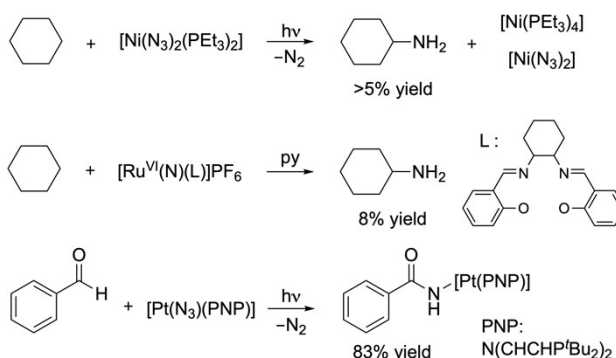
Institut für Anorganische Chemie  
 Universität Göttingen  
 Tammannstraße 4, 37077 Göttingen (Germany)  
 E-mail: sven.schneider@chemie.uni-goettingen.de

H. Verplancke, J. N. Lienert, Prof. M. C. Holthausen  
 Institut für Anorganische und Analytische Chemie  
 Goethe-Universität  
 Max-von-Laue-Straße 7, 60438 Frankfurt am Main (Germany)  
 E-mail: max.holthausen@chemie.uni-frankfurt.de

G. P. Van Trieste, III, K. A. Reid, J. H. Reibenspies, Prof. D. C. Powers  
 Department of Chemistry, Texas A&M University  
 3255 TAMU, College Station, TX 77843 (USA)  
 E-mail: david.powers@chem.tamu.edu

© 2021 The Authors. *Angewandte Chemie International Edition* published by Wiley-VCH GmbH. This is an open access article under the terms of the Creative Commons Attribution Non-Commercial License, which permits use, distribution and reproduction in any medium, provided the original work is properly cited and is not used for commercial purposes.

### Previous Work: Stoichiometric C–H Nitrogen Atom Insertion



### This Work: Catalytic C–H Nitrogen Atom Transfer



**Scheme 1.** Stoichiometric, intermolecular C–H nitrogen atom insertion reactions by (formal) terminal nitride complexes reported in the literature (top), and aldehyde amidation via catalytic C–H *nitrogen atom transfer* reported here (bottom).

competition of insertion and dehydrogenation pathways, as was observed, e.g., for the reaction of a ruthenium(VI) nitride with cycloalkanes.<sup>[11b]</sup> New strategies for selective, intermolecular C–H insertion of nitrides are therefore required to develop hitherto elusive nitrogen atom transfer catalysis.

In recent years, we examined (formal) terminal nitride complexes with nitrenoid character and their nitrogen atom transfer reactivity.<sup>[11d,12]</sup> In the case of the platinum complex [Pt(N)(PNP)] (PNP = N(CHCHP<sup>t</sup>Bu<sub>2</sub>)<sub>2</sub>), photocrystallographic, magnetic, and computational characterization supported the description as authentic {Pt<sup>II</sup>–N} metallonitrene with a monovalent, diradical, atomic nitrogen ligand.<sup>[11d]</sup> This transient species undergoes facile nitride insertion into H–B, C–B, and C–H bonds. Notably, stoichiometric aldehyde amidation (Scheme 1) exhibited a large, positive Hammett reaction parameter and a PhC(O)–H/D kinetic isotope effect (KIE) of unity was found. These observations are consistent with rate-determining, nucleophilic attack of the metallonitrene at the carbonyl group and subsequent intramolecular hydrogen shift over a radical rebound mechanism, despite the moderate C–H bond strength of aldehydes (BDE<sub>gas</sub>(PhC(O)–H) = 89 kcal mol<sup>–1</sup>).<sup>[13]</sup> Computational analysis supported this interpretation. This nucleophilic *nitrogen atom transfer* mechanism for aldehyde amidation exhibits inverted selectivity with respect to the electrophilic *nitrene transfer* (N–R; R = Ts, aryl, alkyl, SiMe<sub>3</sub>) pathways via radical or concerted C–H insertion, which generally feature moderate to large, negative  $\rho$ -values and sizable KIEs.<sup>[14]</sup>

Amide syntheses are the most frequent reactions in pharmaceutical chemistry, and atom economic strategies have been acknowledged as a priority area for synthetic method development.<sup>[15]</sup> N-atom transfer could be an attractive approach towards primary amides. We therefore considered oxidative aldehyde amidation via (formal) terminal nitride C–H insertion as an interesting case to develop catalytic *nitrogen atom transfer* with inverted selectivity. In this contribution, a photocatalytic protocol for silylamidation of aldehydes is reported as a facile route towards primary amides. This first example for *catalytic nitrogen atom transfer* relies on inverted, nucleophilic C–H insertion of a transient palladium(II) metallonitrene and transsilylation as an efficient strategy for product release.

## Results and Discussion

While our previously reported platinum metallonitrene undergoes facile C–H insertion with aldehydes, the resulting amide complex proved inert to product release, which prevented catalytic turnover. For this reason, we moved to palladium, which generally exhibits more rapid substitution kinetics.<sup>[16]</sup> The air-stable palladium(II) azide complex [Pd(N<sub>3</sub>)(PNP)] (**1**) can be synthesized in three steps from the respective chloride with 63 % yield. The structures of **1** and all precursors were confirmed by NMR spectroscopy and single-crystal X-ray diffraction<sup>[17]</sup> and closely resemble those of the analogous platinum complexes. The UV/Vis spectra

of **1** and [Pt(N<sub>3</sub>)(PNP)] in THF (Figure 1b) have similar low-energy edges of the strong near-UV bands, yet with an additional, weaker band for **1** at 393 nm, suggesting azide photolysis with blue light.

In crystallo extrusion of N<sub>2</sub> from **1** enabled the observation and X-ray crystallographic characterization of the formal terminal nitride complex [Pd(N)(PNP)] (**2**, Figure 1a) (see Supporting Information section 5.7).<sup>[18]</sup> Prolonged irradiation ( $\lambda_{\text{exc}} = 365$  nm) of a single crystal at 100 K while collecting X-ray diffraction data (synchrotron radiation;  $\lambda = 0.41328$  Å) resulted in the conversion of **1** to **2** and N<sub>2</sub> (i.e., 2N<sub>2</sub>). The structure of 2N<sub>2</sub> was refined from a crystal with 40 % conversion; sample degradation and ultimately loss of crystallinity was observed upon further conversion. N<sub>2</sub>-elimination is accompanied by a significant contraction of the Pd(1)–N(1) distance from 2.050(2) Å (**1**) to 1.92(2) Å (2N<sub>2</sub>), which is in agreement with the computed model of **2** ( $d_{\text{Pd-N}} = 1.891$  Å, see below). Similar observations were obtained for the platinum analogue (exp:  $\Delta d_{\text{Pt-N}} = 0.16$  Å). The evolved N<sub>2</sub> occupies a void space in the crystal lattice that is generated by Van der Waals packing of the *tert*-butyl substituents and was refined at 28 % occupancy, which is consistent with partial loss from the lattice during the experiment. Similar to previous in crystallo syntheses of metal nitrenoids,<sup>[19,20]</sup> N<sub>2</sub> extrusion can be promoted by sustained exposure to synchrotron radiation; about 10 % conversion of **1** to 2N<sub>2</sub> is observed during simple structure determination of **1** prior to photolysis.

The electronic structure of **2** was examined by magnetic characterization upon in situ photolysis ( $\lambda_{\text{exc}} = 390$  nm) of a microcrystalline sample of **1** inside a superconducting quantum interference device (SQUID) magnetometer at 10 K (Figure 1c) (see Supporting Information section 4). The  $\chi_{\text{m}} T$  product of the photoproduct shows a steep rise at

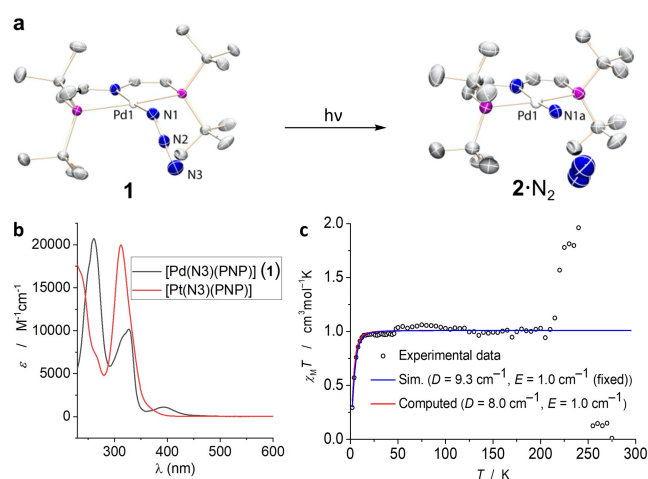


**Figure 1.** a) Displacement ellipsoid plots of **1** and **2** N<sub>2</sub> from in crystallo N<sub>2</sub>-extrusion. **2** N<sub>2</sub> was refined from a sample with 40 % conversion of **1**. Selected bond lengths [Å]: **1** Pd–N1, 2.050(2); **2** N<sub>2</sub> Pd–N1 A, 1.92(2). b) Solution UV/Vis spectra of **1** and the analogous Pt complex in THF. c)  $\chi_{\text{m}} T$  vs.  $T$  data (circles) from in situ photolysis ( $\lambda_{\text{exc}} = 390$  nm) of **1** obtained by SQUID magnetometry with simulated (red) and ab initio computed (blue) values.

low temperatures and reaches a plateau at temperatures below 20 K. The rise of the magnetic moment above 200 K is attributed to the decomposition of the metallonitrene photoproduct. Notably, the maximum magnetic moment of **2** is obtained at considerably lower temperatures, as compared with [Pt(N)(PNP)] (> 120 K), which indicates significantly smaller splitting of the spin microstates. Accordingly, the conversion-normalized magnetic data could be well fitted to a zero-field splitting (ZFS) spin-Hamiltonian for a spin triplet ground state with fixed isotropic  $g$  factor ( $g=2$ ) by using an axial ZFS parameter of  $D=9.3\text{ cm}^{-1}$ , which is about an order of magnitude smaller as compared with [Pt(N)(PNP)] ( $D=85\text{ cm}^{-1}$ ).

Quantum-chemical assessment (ONIOM(CC-F12:DFT)) confirmed the triplet ground-state of **2** with a singlet/triplet gap of  $\Delta E_{S-T}=18\text{ kcal mol}^{-1}$ . Notably, the spin-density is even more nitrogen-centered (96%) as compared to [Pt(N)(PNP)] (91%).<sup>[11d]</sup> Consistently, relativistic CASSCF/NEVPT2/QDPT calculations (see Supporting Information section 6.1) disclose substantially reduced spin-orbit coupling effects on the spin-state energetics and almost negligible splitting of the triplet-microstates ( $D=8\text{ cm}^{-1}$ ), which is in excellent agreement with experiment. The characteristic natural localized molecular orbitals (NLMOs) resulting from a natural bond orbital (NBO) analysis of the ground-state wave function closely resemble the qualitative picture obtained for [Pt(N)(PNP)] with a Pd–N  $\sigma$ -bond, a lone-pair and two singly occupied p-orbitals at the nitrogen, and four non-bonding Pd d-orbitals (Figure 2).

Having confirmed the photochemical metallonitrene formation, C–H amidation of the model substrate benzaldehyde was examined by photolysis (LED, 390 or  $427 \pm 20\text{ nm}$ ) of **1** and PhCHO (1.2 equiv.) at room temperature in benzene. The insertion product [Pd(NHC(O)Ph)(PNP)] (**3**) was obtained after 1 h in quantitative yield (Scheme 2). The quantum yields for the consumption of **1** in the presence and absence of benzaldehyde were identical within error (around 0.1%), which excludes a photoinitiated, thermal radical chain mechanism for the formation of **3**. The decay rate of **1** scales linearly with the photon flux but is independent from

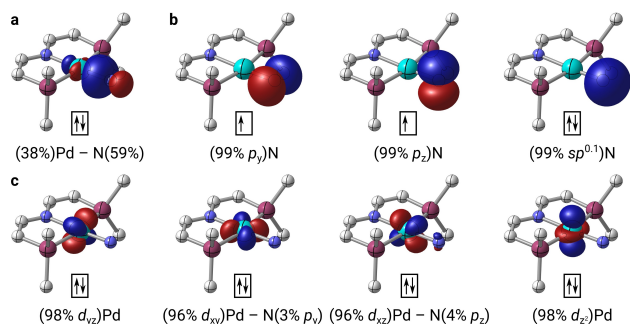
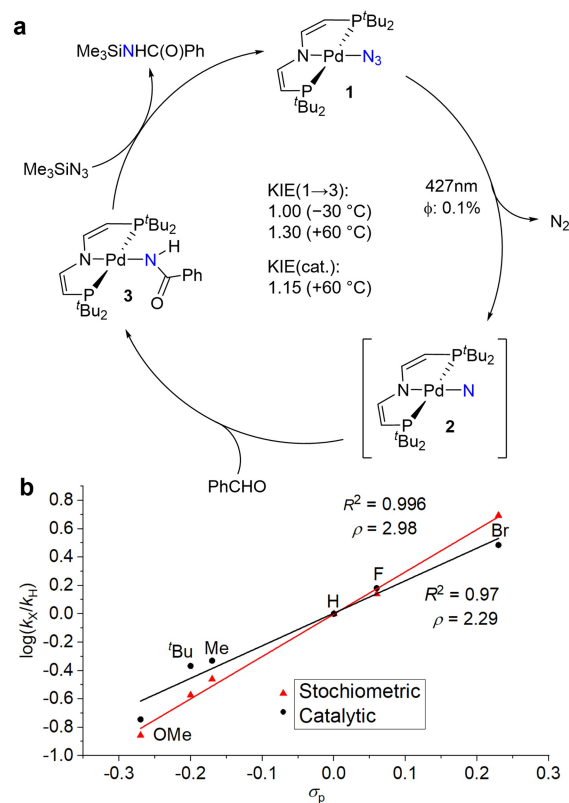


**Figure 2.** Characteristic NLMOs derived by NBO analysis for the Pd–N  $\sigma$ -bond (a), the N-centered singly occupied  $p_x$  and  $p_y$  orbitals and  $s$ -type lone pair (b), and the doubly occupied Pd d-orbitals (c); isosurfaces at  $\pm 0.05\text{ a}_0^{-3/2}$ ; doubly occupied orbitals obtained by spatial averaging over  $\alpha$  and  $\beta$  spin orbitals; methyl groups and hydrogen atoms are omitted for clarity.



**Scheme 2.** a) Proposed catalytic cycle. b) Hammett plots for stoichiometric (**1**→**3**, black; [ArCHO]<sub>0</sub>: [PhCHO]<sub>0</sub>: [I] = 10: 10: 1, 5 min) and catalytic (red; [ArCHO]<sub>0</sub>: [PhCHO]<sub>0</sub>: [I]: [TMSN<sub>3</sub>]<sub>0</sub> = 10: 10: 1: 50, 5 h) amidation of *para*-substituted benzaldehydes (60 °C, C<sub>6</sub>D<sub>6</sub>, 427 nm).

benzaldehyde concentration. Furthermore, the photolysis of **1**/PhCHO (1: 10) in frozen THF (10 h, 82% conversion) and subsequent thawing gave **3** in 32% yield (see Supporting Information section 2.4). These observations are in line with initial, rate-determining photoconversion of **1** to **2** and subsequent reaction of the photoproduct by thermal C–H insertion with the aldehyde. Frozen solution photolysis also gave [PdH(PNP)] (12%). This might originate from Pd<sup>I</sup> radical chemistry due to bimolecular nitrene coupling and N<sub>2</sub> elimination at high steady state concentration of **2**,<sup>[12]</sup> followed by hydrogen atom abstraction from PhCHO or solvent.

Hammett analysis by competition experiments with a range of *para*-substituted benzaldehydes gave a good linear correlation of  $\log(k_X/k_H)$  with substituent parameter  $\sigma_p$  (Scheme 2).<sup>[21]</sup> The reaction parameter ( $\rho = +3.0$  at 60 °C) is close to that of hydroxide addition to benzaldehydes ( $\rho = +2.8$ ),<sup>[22]</sup> which supports nucleophilic attack of the photoproduct at the carbonyl group instead of radical C–H activation or electrophilic insertion via the singlet metallonitrene.<sup>[4,14]</sup> An even steeper slope ( $\rho = +4.4$ ) was obtained for the platinanitrene and attributed to irreversible adduct formation, followed by H-transfer to the nitrogen atom with slightly lower barrier ( $\Delta\Delta G^\ddagger = 3.8\text{ kcal mol}^{-1}$ ).<sup>[11d]</sup> As in that case, an H/D kinetic isotope effect (KIE) near unity was observed upon photolysis of **1** with PhC(O)H/D

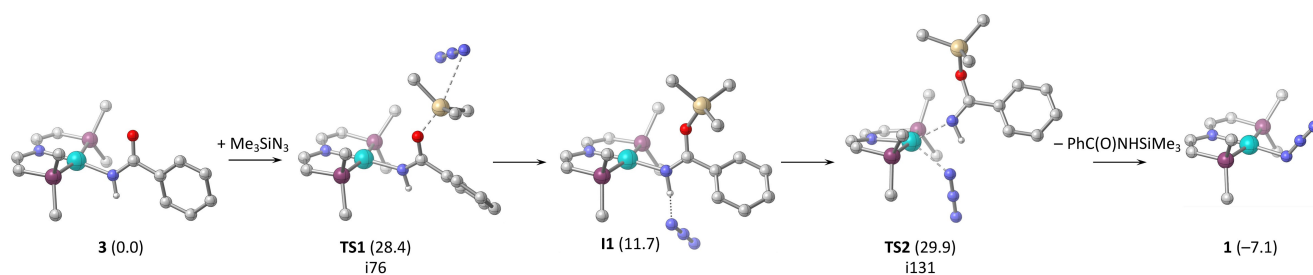


**Figure 3.** Computed pathway for transamidation with  $\Delta G^{333K}$  in kcal mol<sup>-1</sup> in parentheses and transition-state imaginary frequencies in cm<sup>-1</sup>; methyl groups and hydrogen atoms are omitted for clarity.

(1:1) at  $-30^{\circ}\text{C}$ . Notably, a small normal KIE ( $k_{\text{H}}/k_{\text{D}} = 1.30 \pm 0.05$ ) was found at higher temperatures ( $+60^{\circ}\text{C}$ ) (see Supporting Information section 2.3). This is in line with a contribution from the C–H cleavage step at higher temperatures, but a secondary isotope effect from initial adduct formation cannot be excluded.<sup>[23]</sup>

Next, transamidation was evaluated to enable catalysis. Among several inorganic azide sources,  $\text{Me}_3\text{SiN}_3$  proved most effective. Reaction with **3** at  $40^{\circ}\text{C}$  quantitatively regenerated **1** and free  $\text{PhC(O)NHSiMe}_3$  within 16 h (Scheme 2). DFT computations indicated that the lowest energy pathway for transamidation commences with carboxyl silylation (Figure 3).<sup>[24]</sup> The H-bonded ion pair intermediate **II** then undergoes rate-determining substitution at the metal for full silylamide release.<sup>[25]</sup> For comparison, the effective free-energy barrier for transamidation of the Pt analogue was computed  $8 \text{ kcal mol}^{-1}$  higher, which renders this reaction inaccessible at synthetically useful temperatures.<sup>[17]</sup>

Motivated by this two-step sequence for aldehyde amidation, a photocatalytic protocol was developed (Table 1). Photolysis (427 nm) of a mixture of **1**, benzaldehyde and  $\text{Me}_3\text{SiN}_3$  (0.05:1:2.5) at  $30^{\circ}\text{C}$  gave low substrate conversion after 24 h. Raising the temperature resulted in increasing benzaldehyde conversion. Total benzamide yields over 70% were obtained at  $T \geq 60^{\circ}\text{C}$ . Quantitative substrate conversion was obtained within 48 h or by raising the catalyst loading to 10 mol%. With a lower catalyst loading of 2 mol%, 78% conversion was achieved after 48 h, corresponding to a turnover number of 43. Significant rate retardation was observed with lower  $\text{Me}_3\text{SiN}_3$  loadings (1 equiv), confirming turn-over limiting transamidation. However, reduced yields at 50% photon flux suggest that  $\text{N}_2$  elimination also contributes to the rate under these conditions. Accordingly, during catalysis at standard conditions (427 nm, 5 mol% **1**, 2.5 equiv  $\text{Me}_3\text{SiN}_3$ ,  $60^{\circ}\text{C}$ ,  $\text{C}_6\text{D}_6$ ), both **1** and **3** were observed by NMR spectroscopy, and **3** as catalyst afforded comparable yields. In contrast, the use of  $[\text{PdCl}(\text{PNP})]$  gave insignificant conversion.

At higher wavelengths (456 nm), slower amidation rates are obtained, defining a low energy limit for the productive photolysis. In contrast, a black precipitate is formed at  $\lambda \leq 390 \text{ nm}$  accompanied by lower selectivity. This observation is attributed to uncatalyzed photoreactivity of benzaldehyde,<sup>[26]</sup> as confirmed by a control experiment in

**Table 1:** Optimization of the reaction conditions.

$\lambda_{\text{exc}}$ [nm]	$T$ [ $^{\circ}\text{C}$ ]	Solvent	[ <b>1</b> ] [mol %]	$[\text{Me}_3\text{SiN}_3]$ [equiv]	Yield <sup>[a]</sup> (conv.) [%]
427	30	$\text{C}_6\text{D}_6$	5.0	2.5	21 (28)
427	50	$\text{C}_6\text{D}_6$	5.0	2.5	46 (52)
427	60	$\text{C}_6\text{D}_6$	5.0	2.5	71 (81)
427	70	$\text{C}_6\text{D}_6$	5.0	2.5	74 (86)
427	60	$\text{C}_6\text{D}_6$	2.0	2.0	68 (78) <sup>[b]</sup>
427	60	$\text{C}_6\text{D}_6$	5.0	2.5	89 (98) <sup>[b]</sup>
427	60	$\text{C}_6\text{D}_6$	10.0	2.5	87 (98)
427	60	$\text{C}_6\text{D}_6$	5.0	1.0	51 (53)
427 <sup>[c]</sup>	60	$\text{C}_6\text{D}_6$	5.0	2.5	62 (60)
427	60	$\text{C}_6\text{D}_6$	5.0 <sup>[d]</sup>	2.5	77 (81)
427	60	$\text{C}_6\text{D}_6$	5.0 <sup>[e]</sup>	2.5	3 (7)
456	60	$\text{C}_6\text{D}_6$	5.0	2.5	29 (32)
390	60	$\text{C}_6\text{D}_6$	5.0	2.5	78 (100)
427	60	THF- $d_8$	5.0	2.5	76 (90)
427	60	Tol- $d_8$	5.0	2.5	68 (76)
427	60	$\text{CD}_3\text{CN}$	5.0	2.5	21 (45)

[a] <sup>1</sup>H NMR yield/conversion after 24 h. [b] 48 h. [c] 50% photon flux. [d] catalyst: **3**. [e] catalyst:  $[\text{PdCl}(\text{PNP})]$ . Full table in Supporting Information 3.1.

the absence of catalyst. Other weakly coordinating solvents, like THF or toluene, give similar results, while the use of acetonitrile strongly reduced both yield and selectivity.

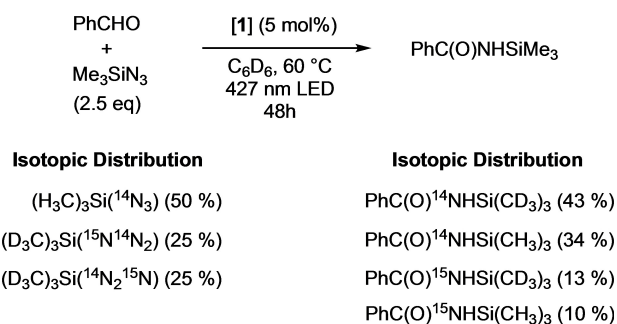
Hammett analysis gave similar relative rates as stoichiometric amidation (Scheme 2). Both the reaction parameter ( $\rho = +2.3$ ) and the KIE ( $k_{\text{H}}/k_{\text{D}} = 1.15 \pm 0.03$ ; see Supporting Information section 2.3) are slightly lower than for the stoichiometric reaction, which is tentatively attributed to a kinetic contribution from the electrophilic transamidation step. These observations support that catalytic nitrogen atom transfer proceeds via the same active species with inverted, nucleophilic selectivity.

Werlé and co-workers recently reported an iron-catalyzed photocatalytic protocol for silylamidation of aromatic and aliphatic aldehydes with  $\text{Me}_3\text{SiN}_3$ .<sup>[14f]</sup> However, in that case more electron-rich aldehydes gave higher yields, which led to the proposal of a nitrenoid  $[\text{Fe}-\text{N}-\text{SiMe}_3]$  intermediate that undergoes electrophilic C–H activation. In order to probe direct trimethylsilylnitrene transfer for the current case, an isotopic cross-labelling experiment was carried out.



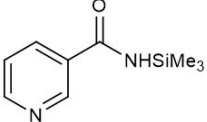
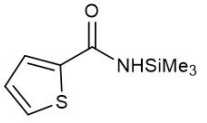
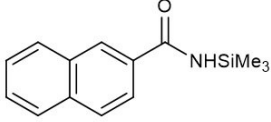
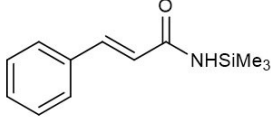
The use of a mixture of  $(\text{CH}_3)_3\text{Si}^{(14}\text{N}_3)$  (50 %),  $(\text{CD}_3)_3\text{Si}^{(14}\text{N}_2^{15}\text{N})$  (25 %), and  $(\text{CD}_3)_3\text{Si}^{(15}\text{N}^{14}\text{N}_2)$  (25 %) as amidation reagent and subsequent analysis by HR-ESI-MS, gave the four possible  $^{14/15}\text{N}$  and  $^{1/2}\text{H}$  isotopologues of trimethylsilylbenzamide in a ratio that is close to the statistical distribution (Scheme 3 and Supporting Information section 2.7). This observation is in line with Si–N cleavage during catalysis, as is inherently the case in a nitride-based but not a nitrene mechanism.

The scope of photocatalytic aldehyde amidation was examined using standard conditions (Table 2). Spectroscopic yields around 60–90 % were obtained for a wide range of donor and acceptor substituted (hetero-)aromatic aldehydes.



**Scheme 3.** Isotopic cross-labelling experiment.

**Table 2:** Substrate scope.

$\text{R}-\text{CHO} + \text{Me}_3\text{SiN}_3 \xrightarrow[\text{48h}]{[\text{1}] (5 \text{ mol}\%), \text{C}_6\text{D}_6, 60^\circ\text{C}, 427 \text{ nm LED}}$ 1.0 eq.      2.5 eq.				$\text{R}-\text{C(O)NHSiMe}_3$	
Products (R)	Yield <sup>[a]</sup> (conv.) (%)				
Ph	89 (98)			 91 (98) %	
2-Me-Ph	91 (99)				
3-Me-Ph	76 (98)				
4-Me-Ph	76 (93)				
4-Ph-Ph	76 (99)				
4-t-Bu-Ph	75 (95)				
4-F-Ph	82 (96)				
4-Br-Ph	44 <sup>[b]</sup> (53)				
4-CO <sub>2</sub> Me-Ph	68 <sup>[b,c]</sup> (99)			 65 (71) %	
4-CF <sub>3</sub> -Ph	59 (76)				
4-Bpin-Ph	56 (83)				
4-NHC(O)CH <sub>3</sub> -Ph	63 <sup>[b,c]</sup> (98)			 78 (98) %	
4-CN-Ph	Trace <sup>[b]</sup> (31)				
<sup>a</sup> Pr	44 (99)				
Ph-CH <sub>2</sub>	49 (99)			 15 (81) %	

[a] <sup>1</sup>H NMR yield/conversion. [b] 24 h. [c] in THF-d<sub>3</sub>.

Deprotection with methanol provides facile access to the respective primary amides. Some substrates gave poor amidation yields, such as *p*-bromobenzaldehyde due to rapid formation of inactive [PdBr(PNP)]. Notably, 2-methylbenzaldehyde gave even higher yields than the *meta*- and *para*-isomers, which might be attributed to sterically enhanced transamidation rates. Rapid conversion, yet poor selectivities were obtained with aliphatic butanal and phenylacetaldehyde. Control experiments for butanal showed unselective photochemical conversion in the absence of catalyst.

## Conclusion

In summary, the synthesis of the first palladium complex with a formal terminal nitride ligand was reported. Photocrystallographic, magnetic and quantum-chemical characterization supports the formulation as an authentic metal-nitrene. The nitrogen-centered biradical character is even more pronounced than in case of the analogous platinum complex, as expressed by much smaller splitting of the spin triplet microstates. Nevertheless, the subvalent nitrogen ligand undergoes facile C–H insertion with aldehydes via nucleophilic, rather than electrophilic or radical attack.

The faster amide transfer kinetics of palladium allowed for the development of a photocatalytic protocol for the oxidative silylamidation of aromatic aldehydes with Me<sub>3</sub>SiN<sub>3</sub>. Product deprotection offers a facile catalytic strategy towards primary amides. Mechanistic analysis by linear free energy relationship, KIE, and isotopic cross-labelling analyses suggest that stoichiometric and catalytic C–H amidation follow the same nucleophilic pathway. Our results emphasize that the use of (formal) nitrides in nitrogen atom transfer catalysis allows for an inversion of the selectivity with respect to typical nitrene transfer catalysis via nitrenoid {M–N–R} species.

## Acknowledgements

S.S. thanks the ERC (CoG Grant 646747) and the DFG (SPP 2102, SCHN950/6-1) for financial support. Quantum-chemical calculations of the Frankfurt group were performed at the Center of Scientific Computing (CSC) Frankfurt on the Goethe-HLR computer cluster. D.C.P. acknowledges the U.S. Department of Energy (DOE), Office of Science, Office of Basic Energy Sciences, Catalysis Program (DE-SC0018977) and the Welch Foundation (A-1907). Yu-Sheng Chen is gratefully acknowledged for assistance in acquiring in crystallo crystallographic data at Sector 15 of the Advanced Photon Source (APS). NSF's ChemMatCARS Sector 15 is supported by the Divisions of Chemistry (CHE) and Materials Research (DMR), National Science Foundation, under grant number NSF/CHE-1834750. Use of the APS, an Office of Science User Facility operated for the U.S. Department of Energy (DOE) Office of Science by Argonne National Laboratory, was supported by the U.S. DOE under Contract No. DE-AC02-

06CH11357. Open Access funding enabled and organized by Projekt DEAL.

### Conflict of Interest

The authors declare no conflict of interest.

### Data Availability Statement

The data that support the findings of this study are available from the corresponding author upon reasonable request.

**Keywords:** Amides · C–H Activation · Nitrenes · Palladium · Photocatalysis

- [1] a) T. Xiong, Q. Zhang, *Chem. Soc. Rev.* **2016**, *45*, 3069–3087; b) Y. Park, Y. Kim, S. Chang, *Chem. Rev.* **2017**, *117*, 9247–9247; c) M. Ju, J. Schomaker, *Nat. Chem. Rev.* **2021**, *5*, 580–594.
- [2] a) P. F. Kuijpers, J. I. van der Vlugt, S. Schneider, B. de Bruin, *Chem. Eur. J.* **2017**, *23*, 13819–13829; b) Y.-C. Wang, X.-J. Lai, K. Huang, S. Yadav, G. Qiu, L. Zhang, H. Zhou, *Org. Chem. Front.* **2021**, *8*, 1677–1693; c) A. Grünwald, S. S. Anjana, D. Munz, *Eur. J. Inorg. Chem.* **2021**, 4147–4166.
- [3] a) S.-M. Au, J.-S. Huang, W.-Y. Yu, W.-H. Fung, C.-M. Che, *J. Am. Chem. Soc.* **1999**, *121*, 9120–9132; b) R. A. Eikey, S. I. Khan, M. M. Abu-Omar, *Angew. Chem. Int. Ed.* **2002**, *41*, 3591–3595; *Angew. Chem.* **2002**, *114*, 3743–3747; c) D. E. Lansky, J. R. Kosack, A. A. Narducci Sarjeant, D. P. Goldberg, *Inorg. Chem.* **2006**, *45*, 8477–8479; d) Y. M. Badieli, A. Dinescu, X. Dai, R. M. Palomino, F. W. Heinemann, T. R. Cundari, T. H. Warren, *Angew. Chem. Int. Ed.* **2008**, *47*, 9961–9964; *Angew. Chem.* **2008**, *120*, 10109–10112; e) E. R. King, E. T. Hennessy, T. A. Betley, *J. Am. Chem. Soc.* **2011**, *133*, 4917–4923; f) V. Lyaskovskyy, A. I. O. Suarez, H. Lu, H. Jiang, X. P. Zhang, B. de Bruin, *J. Am. Chem. Soc.* **2011**, *133*, 12264–12273; g) S. Kundu, E. Miceli, E. Farquhar, F. F. Pfaff, U. Kuhlmann, P. Hildebrandt, B. Braun, C. Greco, K. Ray, *J. Am. Chem. Soc.* **2012**, *134*, 14710–14713; h) F. Dielmann, D. M. Andrada, G. Frenking, G. Bertrand, *J. Am. Chem. Soc.* **2014**, *136*, 3800–3802; i) A. Grünwald, N. Orth, A. Scheurer, A. Pöthig, F. W. Heinemann, D. Munz, *Angew. Chem. Int. Ed.* **2018**, *57*, 16228–16232; *Angew. Chem.* **2018**, *130*, 16463–16467; j) K. M. Carsch, I. M. DiMucci, D. A. Iovan, A. Li, S.-L. Zheng, C. J. Titus, S. J. Lee, K. D. Irwin, D. Nordlund, K. M. Lancaster, T. A. Betley, *Science* **2019**, *365*, 1138–1143; k) H. Shi, J. Xie, W. W. Y. Lam, W.-L. Man, C.-K. Mak, S.-M. Yiu, H. K. Lee, T.-C. Lau, *Chem. Eur. J.* **2019**, *25*, 12895–12899.
- [4] a) I. Nägeli, C. Baud, G. Bernardinelli, Y. Jacquier, M. Moran, P. Müller, *Helv. Chim. Acta* **1997**, *80*, 1087–1105; b) S. K.-Y. Leung, W.-M. Tsui, J.-S. Huang, C.-M. Che, J.-L. Liang, N. Zhu, *J. Am. Chem. Soc.* **2005**, *127*, 16629–16640; c) K. W. Fiori, J. Du Bois, *J. Am. Chem. Soc.* **2007**, *129*, 562–568; d) M. E. Harvey, D. G. Musaev, J. Du Bois, *J. Am. Chem. Soc.* **2011**, *133*, 17207–17216; e) S. M. Paradine, J. R. Griffin, J. Zhao, A. L. Petronico, S. M. Miller, M. C. White, *Nat. Chem.* **2015**, *7*, 987–994; f) S. Hong, K. D. Sutherlin, A. K. Vardhaman, J. J. Yan, S. Park, Y.-M. Lee, S. Jang, X. Lu, T. Ohta, T. Ogura et al., *J. Am. Chem. Soc.* **2017**, *139*, 8800–8803; g) C. Weatherly, J. M. Alderson, J. F. Berry, J. E. Hein, J. M. Schomaker, *Organometallics* **2017**, *36*, 1649–1661; h) L.-M. Jin, P. Xu, J. Xie, X. P. Zhang, *J. Am. Chem. Soc.* **2020**, *142*, 20828–20836.
- [5] The Driver group observed a V-shaped Hammett correlation for plotting the rates of Rh-catalyzed conversion of *ortho*-biaryl azides to carbazoles vs.  $\sigma^+$ . The positive reaction parameter for highly electron withdrawing substituents was attributed to a change in mechanism: B. J. Stokes, K. J. Richert, T. G. Driver, *J. Org. Chem.* **2009**, *74*, 6442–6451.
- [6] J. Du Bois, C. S. Tomooka, J. Hong, E. M. Carreira, *Acc. Chem. Res.* **1997**, *30*, 364–372.
- [7] Y. Liu, T.-C. Lau, *J. Am. Chem. Soc.* **2019**, *141*, 3755–3766.
- [8] a) J. T. Groves, T. Takahashi, *J. Am. Chem. Soc.* **1983**, *105*, 2073–2074; b) S. Minakata, T. Ando, M. Nishimura, I. Ryu, M. Komatsu, *Angew. Chem. Int. Ed.* **1998**, *37*, 3392–3394; *Angew. Chem.* **1998**, *110*, 3596–3598; c) S. N. Brown, *J. Am. Chem. Soc.* **1999**, *121*, 9752–9753; d) A. G. Maestri, K. S. Cherry, J. J. Toboni, S. N. Brown, *J. Am. Chem. Soc.* **2001**, *123*, 7459–7460; e) S. K.-Y. Leung, J.-S. Huang, J.-L. Liang, C.-M. Che, Z.-Y. Zhou, *Angew. Chem. Int. Ed.* **2003**, *42*, 340–343; *Angew. Chem.* **2003**, *115*, 354–357; f) A. G. Maestri, S. D. Taylor, S. M. Schuck, S. N. Brown, *Organometallics* **2004**, *23*, 1932–1946; g) W.-L. Man, W. W. Y. Lam, S.-M. Yiu, T.-C. Lau, S.-M. Peng, *J. Am. Chem. Soc.* **2004**, *126*, 15336–15337; h) W.-L. Man, J. Xie, P.-K. Lo, W. W. Y. Lam, S.-M. You, K.-C. Lau, T.-C. Lau, *Angew. Chem. Int. Ed.* **2014**, *53*, 8463–8466; *Angew. Chem.* **2014**, *126*, 8603–8606; i) S. B. Muñoz III, W.-T. Lee, D. A. Dickie, J. J. Scepaniak, D. Subedi, M. Pink, M. D. Johnson, J. M. Smith, *Angew. Chem. Int. Ed.* **2015**, *54*, 10600–10603; *Angew. Chem.* **2015**, *127*, 10746–10749; j) J. Xie, W.-L. Man, C.-Y. Wong, X. Chang, C.-M. Che, T.-C. Lau, *J. Am. Chem. Soc.* **2016**, *138*, 5817–5820; k) D. W. Crandell, S. B. Muñoz III, J. M. Smith, M.-H. Baik, *Chem. Sci.* **2018**, *9*, 8542–8552.
- [9] a) Nitride C–H insertion in the gas phase: S. Zhou, J. Li, M. Schlangen, H. Schwarz, *Angew. Chem. Int. Ed.* **2016**, *55*, 14863–14866; *Angew. Chem.* **2016**, *128*, 15085–15089; b) S. Zhou, X. Sun, L. Yue, C. Guo, M. Schlangen, H. Schwarz, *Angew. Chem. Int. Ed.* **2018**, *57*, 15902–15906; *Angew. Chem.* **2018**, *130*, 16129–16133.
- [10] Intramolecular nitride C–H insertion: a) C. C. Hojilla Atienza, A. C. Bowman, E. Lobkovsky, P. J. Chirik, *J. Am. Chem. Soc.* **2010**, *132*, 16343–16345; b) R. K. Thomson, T. Cantat, B. L. Scott, D. E. Morris, E. R. Batista, J. L. Kiplinger, *Nat. Chem.* **2010**, *2*, 723–729; c) J. Schöffel, N. Šušnjari, S. Nüchel, D. Sieh, P. Burger, *Eur. J. Inorg. Chem.* **2010**, 4911–4915; d) A. K. M. Long, G. H. Timmer, J. S. Pap, J. L. Snyder, R. P. Yu, J. F. Berry, *J. Am. Chem. Soc.* **2011**, *133*, 13138–13150; e) D. M. King, F. Tuna, E. J. L. McInnes, J. McMaster, W. Lewis, A. J. Blake, S. T. Liddle, *Nat. Chem.* **2013**, *5*, 482–488; f) P. Cui, Q. Wang, S. P. McCollom, B. C. Manor, P. J. Carroll, N. C. Tomson, *Angew. Chem. Int. Ed.* **2017**, *56*, 15979–15983; *Angew. Chem.* **2017**, *129*, 16195–16199; g) J. Ghannam, Z. Sun, T. R. Cundari, M. Zeller, A. Lugosan, C. M. Stanek, W.-T. Lee, *Inorg. Chem.* **2019**, *58*, 7131–7135.
- [11] Intermolecular nitride C–H insertion: a) H. Henning, K. Hofbauer, K. Handke, R. Stich, *Angew. Chem. Int. Ed. Engl.* **1997**, *36*, 408–410; *Angew. Chem.* **1997**, *109*, 373–375; b) W.-L. Man, W. W. Y. Lam, H.-K. Kwong, S.-M. Yiu, T.-C. Lau, *Angew. Chem. Int. Ed.* **2012**, *51*, 9101–9104; *Angew. Chem.* **2012**, *124*, 9235–9238; c) C.-H. Wang, A. Das, W.-Y. Gao, D. C. Powers, *Angew. Chem. Int. Ed.* **2018**, *57*, 3676–3681; *Angew. Chem.* **2018**, *130*, 3738–3743; d) J. Sun, J. Abbenseth, H. Verplancke, M. Diefenbach, B. de Bruin, D. Hunger, C. Würtele, J. van Slageren, M. C. Holthausen, S. Schneider, *Nat. Chem.* **2020**, *12*, 1054–1059.
- [12] a) M. G. Scheibel, B. Askevold, F. Heinemann, E. I. Reijerse, B. de Bruin, S. Schneider, *Nat. Chem.* **2012**, *4*, 552–558; b) M. G. Scheibel, Y. Wu, A. C. Stückl, L. Krause, E. Carl, D. Stalke, B. de Bruin, S. Schneider, *J. Am. Chem. Soc.* **2013**, *135*,

- 17719–17722; c) M. G. Scheibel, J. Abbenseth, M. Kinauer, F. W. Heinemann, C. Würtele, B. de Bruin, S. Schneider, *Inorg. Chem.* **2015**, *54*, 9290–9302; d) J. Abbenseth, M. Finger, C. Würtele, M. Kasanmascheff, S. Schneider, *Inorg. Chem. Front.* **2016**, *3*, 469–477.
- [13] J. A. Martinho Simões, D. Griller, *Chem. Phys. Lett.* **1989**, *158*, 175–177.
- [14] a) J. W. W. Chang, P. W. H. Chan, *Angew. Chem. Int. Ed.* **2008**, *47*, 1138–1140; *Angew. Chem.* **2008**, *120*, 1154–1156; b) J. W. W. Chang, T. M. U. Ton, S. Tania, P. C. Taylor, P. W. H. Chan, *Chem. Commun.* **2010**, *46*, 922–924; c) T. M. U. Ton, C. Tejo, S. Tania, J. W. W. Chang, P. W. H. Chan, *J. Org. Chem.* **2011**, *76*, 4894–4904; d) B. Zhou, Y. Yang, J. Shi, H. Feng, Y. Li, *Chem. Eur. J.* **2013**, *19*, 10511–10515; e) L.-M. Jin, H. Lu, Y. Cui, C. L. Lizardi, T. N. Arzua, L. Wojtas, X. Cui, X. P. Zhang, *Chem. Sci.* **2014**, *5*, 2422–2427; f) B. Chatterjee, S. Jena, V. Chugh, T. Weyhermüller, C. Werlé, *ACS Catal.* **2021**, *11*, 7176–7185.
- [15] a) D. G. Brown, J. Boström, *J. Med. Chem.* **2016**, *59*, 4443–4458; b) M. T. Sabatini, L. T. Boulton, H. F. Sneddon, T. D. Sheppard, *Nat. Catal.* **2019**, *2*, 10–17.
- [16] Ž. D. Bugarčić, J. Bogojeski, R. van Eldik, *Coord. Chem. Rev.* **2015**, *292*, 91–106.
- [17] See Supporting Information for synthetic, catalytic, spectroscopic, crystallographic and computational details.
- [18] a) J. M. Cole, *Chem. Soc. Rev.* **2004**, *33*, 501–513; b) A. Das, G. P. van Trieste III, D. C. Powers, *Comments Inorg. Chem.* **2020**, *40*, 116–158.
- [19] a) A. Das, C.-H. Wang, G. P. van Trieste III, C.-J. Sun, Y.-S. Chen, J. H. Reibenspies, D. C. Powers, *J. Am. Chem. Soc.* **2020**, *142*, 19862–19867; b) A. Das, Y.-S. Chen, J. H. Reibenspies, D. C. Powers, *J. Am. Chem. Soc.* **2019**, *141*, 16232–16236.
- [20] Y. Baek, A. Das, S.-L. Zheng, J. H. Reibenspies, D. C. Powers, T. A. Betley, *J. Am. Chem. Soc.* **2020**, *142*, 11232–11243.
- [21] C. Hansch, A. Leo, R. W. Taft, *Chem. Rev.* **1991**, *91*, 165–195.
- [22] A. Williams, *Free energy relationships in organic and bio-organic chemistry*, 1st ed., Royal Society of Chemistry, Cambridge, **2003**.
- [23] a) For C–H  $sp^2$  to  $sp^3$  rehybridization, inverse isotope effects are generally expected in the low temperature limit based on the the zero-point energy contribution. However, the temperature dependence of isotope effects can be complicated. See: J. Bigeleisen, M. W. Lee, F. Mandel, *Annu. Rev. Phys. Chem.* **1973**, *24*, 407–440; b) G. Parkin, *Acc. Chem. Res.* **2009**, *42*, 315–325.
- [24] a) Molecular structures and thermal/vibrational contributions to Gibbs free energies were obtained at the PBE0-D/def2-SVP level of DFT. PBE0-D/def2-TZVPP single point calculations employing the SMD solvent model were used for improved energies (SMD(Benzene)-PBE0-D/def2-TZVPP). To cope with the reduction of the particle count ( $A+B \rightarrow C$ ) a standard-state correction term of  $-2.12 \text{ kcal mol}^{-1}$  was included in the relative free energies. See Supporting Information for further details. PBE0 density functional: J. P. Perdew, M. Ernzerhof, K. Burke, *J. Chem. Phys.* **1996**, *105*, 9982–9985; b) C. Adamo, V. Barone, *J. Chem. Phys.* **1999**, *110*, 6158–6170; c) def-2 basis sets; F. Weigend, R. Ahlrichs, *Phys. Chem. Chem. Phys.* **2005**, *7*, 3297–3305; d) SMD solvent model: A. V. Marenich, C. J. Cramer, D. G. Truhlar, *J. Phys. Chem. B* **2009**, *113*, 6378–6396; e) Gaussian software package: Gaussian 16, Revision C.01, M. J. Frisch, G. W. Trucks, H. B. Schlegel, G. E. Scuseria, M. A. Robb, J. R. Cheeseman, G. Scalmani, V. Barone, G. A. Petersson, H. Nakatsuji, X. Li, M. Caricato, A. V. Marenich, J. Bloino, B. G. Janesko, R. Gomperts, B. Mennucci, H. P. Hratchian, J. V. Ortiz, A. F. Izmaylov, J. L. Sonnenberg, D. Williams-Young, F. Ding, F. Lipparini, F. Egidi, J. Goings, B. Peng, A. Petrone, T. Henderson, D. Ranasinghe, V. G. Zakrzewski, J. Gao, N. Rega, G. Zheng, W. Liang, M. Hada, M. Ehara, K. Toyota, R. Fukuda, J. Hasegawa, M. Ishida, T. Nakajima, Y. Honda, O. Kitao, H. Nakai, T. Vreven, K. Throssell, J. A. Montgomery, J. E. Peralta, F. Ogliaro, M. J. Bearpark, J. J. Heyd, E. N. Brothers, K. N. Kudin, V. N. Staroverov, T. A. Keith, R. Kobayashi, J. Normand, K. Raghavachari, A. P. Rendell, J. C. Burant, S. S. Iyengar, J. Tomasi, M. Cossi, J. M. Millam, M. Klene, C. Adamo, R. Cammi, J. W. Ochterski, R. L. Martin, K. Morokuma, O. Farkas, J. B. Foresman, D. J. Fox, **2016** Wallingford CT: Gaussian, Inc.
- [25] The activation barrier is an upper bound, as computed gas phase entropic contributions in solution are overestimated in our calculations. A lower bound of  $27 \text{ kcal mol}^{-1}$  can be estimated by calculating the activation free energy relative to the loosely associated reactants, **3** and  $\text{Me}_3\text{SiN}_3$ , as a supermolecule; J. Song, E. L. Klein, F. Neese, S. Ye, *Inorg. Chem.* **2014**, *53*, 7500–7507.
- [26] M. A. Theodoropoulou, N. F. Nikitas, C. G. Kokotos, *Beilstein J. Org. Chem.* **2020**, *16*, 833–857.

Manuscript received: November 16, 2021

Accepted manuscript online: December 14, 2021

Version of record online: January 14, 2022